Aeroacoustic Analysis of a NACA Duct

Nicolas J. Pignier, Ciarán J. O'Reilly, Susann Boij
The Centre for ECO^2 Vehicle Design at KTH, Teknikringen 8, 100 44 Stockholm, Sweden.
KTH Royal Institute of Technology, Department of Aeronautical and Vehicle Engineering, Teknikringen 8, 100 44 Stockholm, Sweden.

Jeremy A. Dahan
Linné Flow Centre at KTH, KTH Royal Institute of Technology, Department of Aeronautical and Vehicle Engineering, Teknikringen 8, 100 44 Stockholm, Sweden.

Summary
An initial aeroacoustic study of a typical NACA inlet is presented. In this paper, the shape of the NACA inlet is based on the experimental work of the National Advisory Committee for Aeronautics. The study is performed at low Mach numbers. A time-averaged solution is obtained through a RANS simulation and validated against experimental results. The results show good agreement both in terms of overall performance of the inlet and in terms of local surface pressures. From the steady simulations, a broadband noise source model is applied to get an estimate of the location of the noise source regions on the surface of the inlet. This model of the NACA inlet will be used for a future acoustic analysis based on unsteady detached eddy simulation (DES) of the flow and on the Ffwocs Williams-Hawkings integral.

PACS no. 43.28.+h, 47.85.Gj

1. Introduction

NACA inlets, also called NACA ducts, are a commonly used type of submerged air inlet that has found application on many types of air and ground vehicles. Developed by the National Advisory Committee for Aeronautics (NACA) in the 1940s [1, 2], they were designed to efficiently draw air from the outside to the inside of a vehicle, providing fresh air that can be used, for instance, in heating, ventilating, and air conditioning systems. Their submerged shape has the advantage of adding only a little additional drag to the vehicle, while providing a design-friendly way to get air into the vehicle compartments. Nowadays, NACA ducts can be found on many types of vehicles, both on ground and air vehicles. Their standard design follows the guidelines provided by the previously mentioned NACA reports. Despite their extensive use in the transport industry, few research papers have been published since the mid-twentieth century. Recently, a couple of numerical studies have investigated the physics of the flow [3, 4], with the aim of designing aerodynamically optimized inlets [5, 6]. These studies provide some insight into the flow that complement the early experimental work by NACA. Recent observations have indicated that NACA inlets could be a considerable source of noise when placed on a vehicle at specific operating conditions. However, the literature on the subject is very scarce. Airbus developed a model of silent NACA inlets aimed at reducing noise in *stationary* operation [7], when external air is actively sucked into the duct. Here, we focus our study on a NACA inlet fixed on a moving vehicle. The overall goal of the project is to develop a NACA inlet which is both aerodynamically and aeroacoustically optimized. In this paper, an initial study is presented, which aims at validating the model for steady flow using Reynolds-averaged Navier-Stokes (RANS) simulations. First acoustic estimations are shown, resulting from the application of a broadband noise source model on the RANS simulations. Later on, unsteady detached eddy simulations (DES) of the flow will be performed on the same NACA inlet, and coupled to a Ffowcs Williams-Hawkings (FW-H) integral [8] to get the far-field noise.
This paper is organized as follows. In the first section, the geometry of the NACA inlet and the methods for the flow and the broadband noise are presented. In the second section, results from the RANS simulations are shown and compared to experimental measurements; results for the broadband noise model are also given. Conclusions and next steps for the project are presented in the last section.

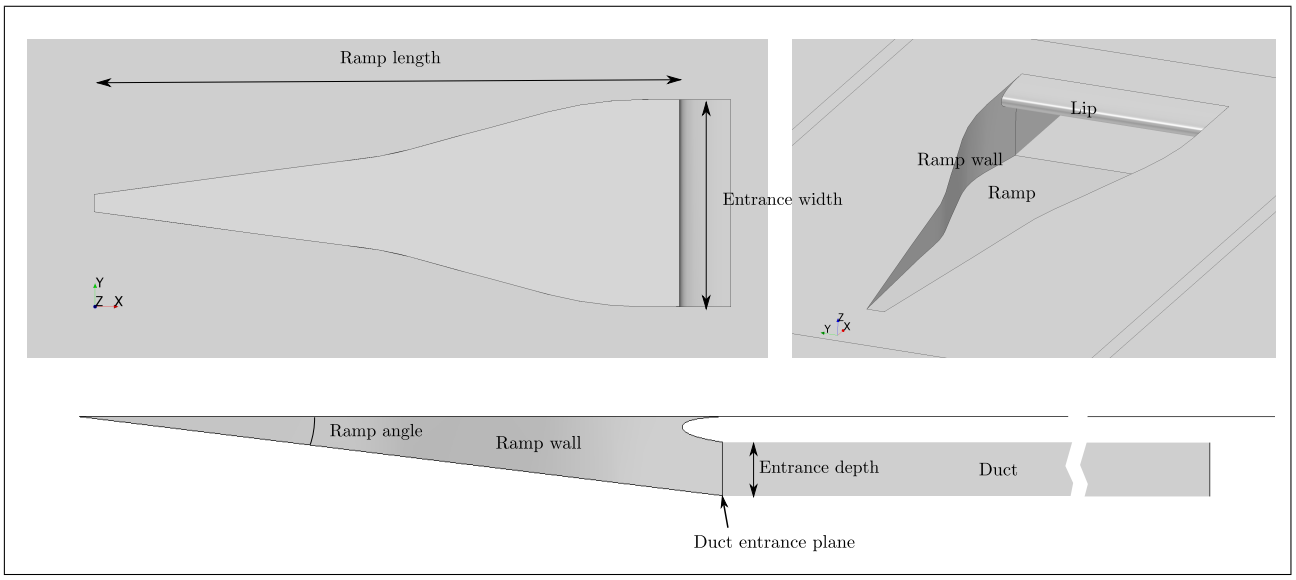

Figure 1. Model of NACA inlet used in the computations.

2. Method

2.1. Model description

The NACA inlet studied in this paper is shown in Figure 1. Its design is based on one of the submerged inlets studied by Mossman *et al.* [2] in wind tunnel tests. The measurements were made on a test inlet for which the shape could be changed according to four main design characteristics: the ramp angle, the curvature of the ramp walls, the lip shape and the width to depth ratio. In the conditions of the experiment, a set of design parameters was identified as being optimal. This optimal inlet had curved diverging ramp walls, a 5° to 7° ramp angle and a width-to-depth ratio of 3 to 5. The submerged inlet that we simulated is a reproduction of this optimal inlet. The external dimensions of the simulated inlet match the ones of the experimental inlet; the only noticeable difference can be found in the duct section downstream of the inlet entrance plane. The experimental duct transitions from a constant rectangular section duct to a circular section diffuser as can be seen in Figure 2. Our model uses only the rectangular duct. Nevertheless, the absence of diffuser in the simulated model is not expected to be a source of error as the experimental results used for validation were measured upstream of the diffuser.

2.2. Fluid dynamic model

The RANS simulations were run on the commercial software STAR-CCM+ [9] in its release 9.06. Two turbulence models were tested: the Spalart-Allmaras model [10] and the SST $k-\omega$ model [11]. The Spalart-Allmaras model is well-known for its simplicity of formulation and its fast and robust convergence. The SST $k-\omega$ model was chosen for its ability to have the accuracy of the $k-\omega$ model in boundary layers while avoiding its sensitivity to free stream boundary conditions by switching to a $k-\epsilon$ model far from the walls. The simulations were run in compressible mode. No significant increase of the computational time was observed between incompressible and compressible simulations. The Reynolds number based on the entrance depth of the duct is around 10^5.

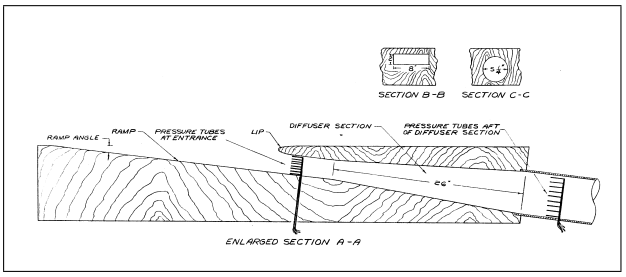

Figure 2. Experimental model and apparatus used by NACA [2].

2.3. Broadband noise source model

To perform an early analysis of the acoustic field generated by the inlet from the RANS simulations, a broadband noise model was used. The model that was used is the one implemented in Star-CCM+ that estimates the broadband acoustic power of Curle's sources, on the surface of the inlet. This model is based on a semi-empirical formula to estimate the pressure fluctuations derivative from the wall-shear stress, the free-stream density, the turbulent kinetic energy, the turbulent time scale and the turbulent length scale. For more details about this method, the reader is referred to the documentation of Star-CCM+ [9] and to Hinze's book [12].

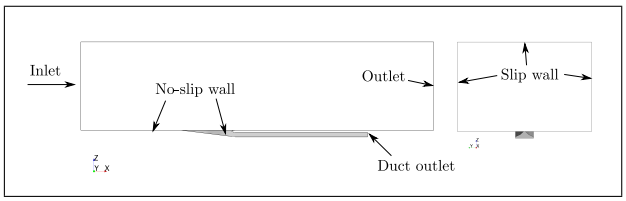

Figure 3. Domain and boundary conditions.

2.4. Computational domain, grid and boundary conditions

The NACA inlet described in Figure 1 is placed in a wind tunnel-type configuration as shown in Figure 3.

Boundary conditions and initial conditions At the inlet, a constant velocity of 60 m/s in the x-direction is imposed. A pressure outlet boundary condition is used at the outlet, the pressure being set to 101325 Pa. The floor of the domain, the surface of the NACA inlet as well as the surface of the duct are modelled as no-slip walls, whereas the walls of the wind-tunnel are modelled as slip walls. At the duct outlet, the pressure is prescribed, through a targeted mass-flow. On this boundary, the solver essentially adjusts the prescribed value of pressure to reach the targeted mass flow during the simulation. Regarding the turbulence models, the turbulent viscosity ratio is set to 200. The length of the domain upstream of the NACA inlet could be adjusted to get the correct boundary layer thickness at the position of the NACA inlet entrance.

Mesh The mesh was generated in Star-CCM+, using trimmed cells on top of a prism layer. The prism layer covers all the no-slip walls and was adjusted to ensure a $y+$ value slightly below 1 on these walls. Volumetric controls were used in the vicinity of the NACA inlet to refine the mesh locally. These controls are shown in Figure 4 and their corresponding mesh size in Table I.

A mesh of 55 M cells was also tested, and no significant difference was observed; the results are therefore presented for the 13.2 M cells mesh.

3. Results

3.1. Analysis of steady RANS simulations

Boundary layer It was shown by Mossman that the boundary layer thickness - more specifically its ratio with the entrance depth - can have a significant impact on the efficiency of the inlet [2]. In order to validate our simulations against the experiments, it is thus important to ensure that the boundary layer correctly matches the experimental one. The boundary layer velocity profile at the location of the duct entrance is shown in Figure 6. This profile is extracted from a simulation in the same domain as presented in Figure 3, but without the NACA inlet.

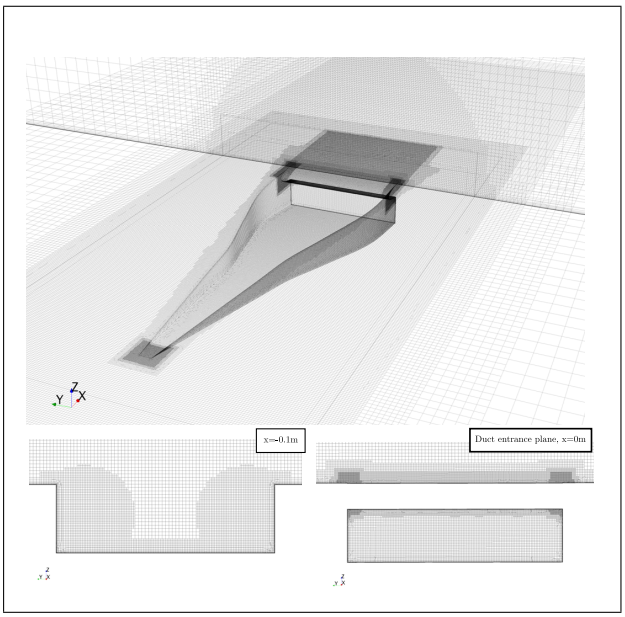

Figure 5. Mesh.

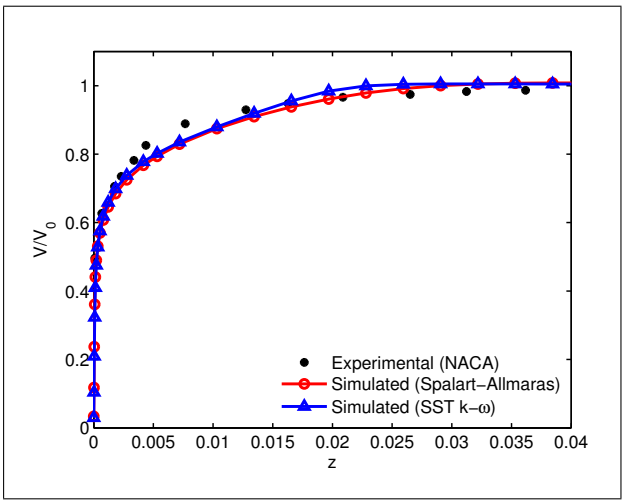

Figure 6. Boundary layer profile at the location of the duct entrance.

Ram recovery ratio NACA introduced the ram recovery ratio as a mean to estimate the performance of a given submerged inlet, and defined it as the ratio of dynamic pressure between the duct entrance and the free stream. The ram recovery ratio is given by

$$\texttt{ram recovery ratio} = \frac{P_{T,1} - p_0}{P_{T,0} - p_0}, \qquad (1)$$

where $P_{T,0}$ and $P_{T,1}$ are the total pressure measured respectively in the free stream and at the entrance plane (averaged over the section for the latter), and where p_0 is the static pressure of the free stream. The ram recovery ratio is represented on Figure 7 as a function of the inlet velocity ratio, defined by the ratio between the averaged velocity at the entrance plane and the free stream velocity V_1/V_0. NACA data

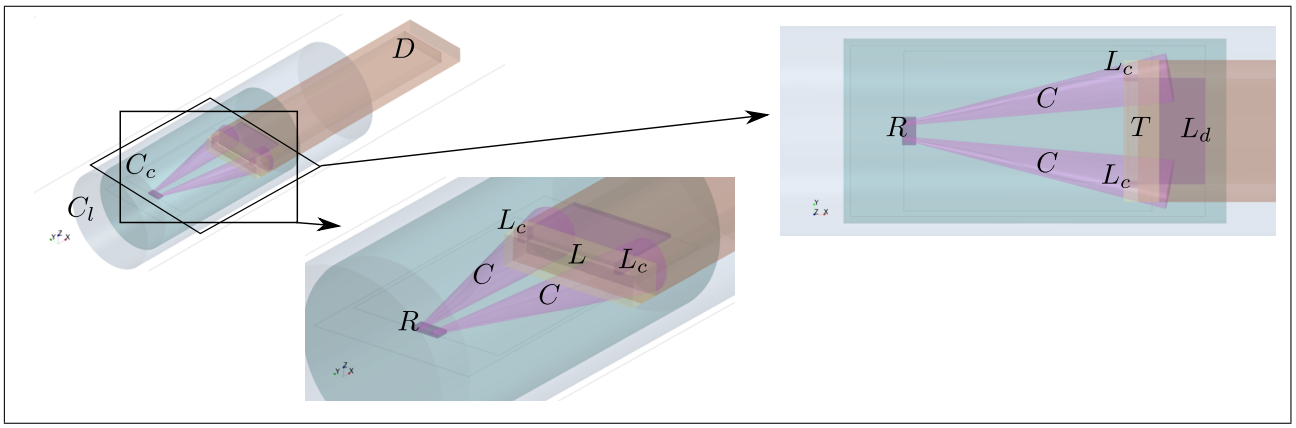

Figure 4. Volumetric controls.

Table I. Volumetric controls and associated cell size.

Volume	$\mathcal{C}_l$	$\mathcal{C}_c$	$\mathcal{D}$	$\mathcal{C}$	$\mathcal{L}$	$\mathcal{L}_c$, $\mathcal{R}$	$\mathcal{T}$	$\mathcal{L}_d$	Total number of cells
Cell size (mm)	10	5	25	2	1	0.5	2	1	13.2M

were measured for a free stream speed V_0 between 55 m/s and 80 m/s, our results were obtained for $V_0 = 60$ m/s. The results are in good agreement, with a maximum error of around 5%. For decreasing velocity ratios from 1 down to 0.4, the ram recovery ratio increases, a trend that is well reproduced by the simulations. The overall over-prediction of the ram recovery ratio could be explained by the imperfect match in boundary layer thickness between the simulated and experimental cases. Mossman showed that a thickened boundary layer can trigger a loss of ram recovery ratio of 0.12 [2]. A closer match of the ram recovery ratio could certainly be obtained by further adjustment of the boundary layer. Another explanation could be the difference in shape of the duct downstream of the duct entrance. Convergence was not obtained for velocity ratios below 0.4, therefore we cannot draw conclusions for this regime at this stage.

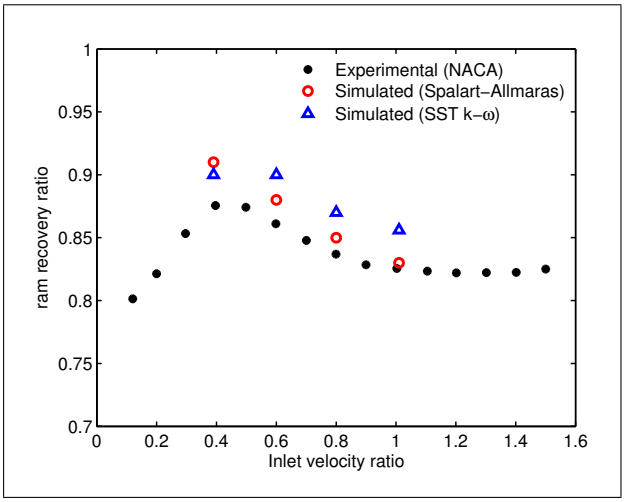

Figure 7. Ram recovery ratio vs inlet velocity ratio.

Flow An example of the surface pressure and streamlines of the flow is shown in Figure 8 for an inlet velocity ratio of $V_1/V_0 = 0.6$. As it is well-known for this type of inlets, the flow is characterized by the counter rotating vortices that are created at the sharp edges between the ramp walls and the external surface. These vortices impinge on the sides of the lip, resulting in part of the flow being drown inside the duct and part of it being dragged with the external flow, the proportion of which depends on the inlet velocity ratio: the lower the inlet velocity ratio, the higher the pressure inside the duct and the less air coming in. In view of this complex flow around the lip, it seems reasonable to think that the main noise sources should be located in this area. A characteristic frequency of around 1000 Hz can be associated with the vortices, based on their length and velocity scales. Assuming that the vortices are the phenomenon from which the noise originates, *i.e.* that they are causing directly or indirectly the pressure fluctuations on the surface, we may expect this frequency to play a particular role in the noise generated.

Pressure coefficient on the inlet surface As the noise emitted by the inlet is our point of focus, it is important to predict the values of surface pressure accurately. In terms of acoustics, the pressure fluctuations matter more than the mean pressure values, but a first step is to verify that the latter are well predicted in the RANS simulation. The pressure coefficient along the ramp and on the lip are represented for various inlet velocity ratio respectively in Figures 9 and 10. The results are shown for both the Spalart-Allmaras and the SST $k-\omega$ turbulence models. The

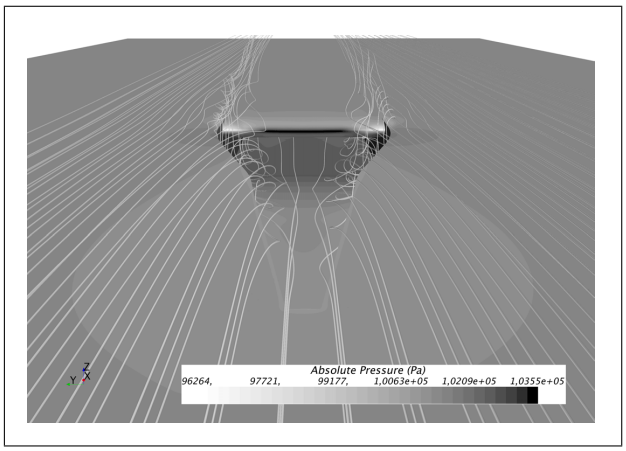

Figure 8. Surface pressure and streamlines for $V_1/V_0 = 0.6$

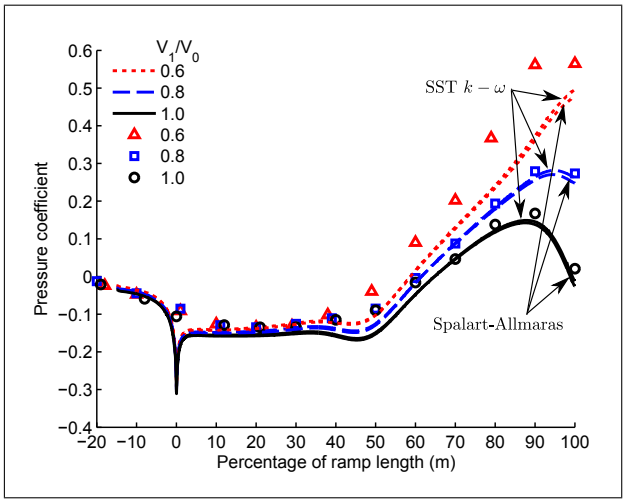

Figure 9. Pressure coefficient distribution along the ramp for various velocity ratio, for the Spalart-Allmaras and the SST $k-\omega$ turbulence models. The lines represent simulated data, the points experimental values [2].

values are extracted in the $y = 0$ plane, that is the symmetry plane of the inlet.

The pressure over the lip is very well predicted for the three velocity ratios. The pressure along the ramp is overall correctly predicted: it is approximately constant in the first half of the ramp and increases in the second half. The slope of this increase gets lower with a higher inlet velocity ratio and this trend is well predicted. A local drop in pressure can be observed at the starting point of the ramp in the simulated data. This is probably due to the sharp transition between the 0° external wall and the 7° ramp on the simulated model, which must have been rounded on the experimental inlet.

3.2. Broadband noise sources results

The broadband noise sources on the surface of the inlet are represented in Figure 11. These results were obtained based on the RANS solutions of the flow with the SST $k-\omega$ turbulence model. According to

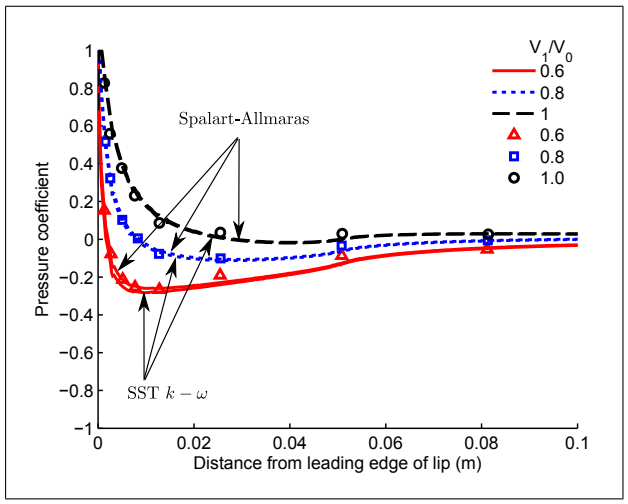

Figure 10. Pressure distribution over the lip for various velocity ratio, for the Spalart-Allmaras and the SST $k-\omega$ turbulence models. NACA for speeds between 55 and 80 m/s, simulated for speed 44.4 m/s. The lines represent simulated data, the points experimental values [2].

these results, the main noise sources would be located on the lip, with strong disturbances at the position of impact of the vortices. The strength of the source seems to increase with decreasing velocity ratio, corresponding to situations where the vortices impact in larger extent on the lip.

4. Conclusion

An initial aeroacoustic analysis of a NACA inlet has been led. RANS simulations of the flow were performed and assessed against experimental data, showing good agreement. The model and the simulation process have thus been validated, and can be used with confidence to predict the flow over various shapes of NACA inlet.

First acoustic estimations could be drawn from a broadband noise source model. From these results it seems that the sources are potentially mainly localized on the lip of the inlet, with maximal values at the location where the vortices created at the ramp wall edges impinge on the lip.

This preliminary study has built a solid foundation for a more thorough acoustic analysis based on unsteady simulations.

Acknowledgement

The work presented here is part of the project: "Noise Propagation from Sustainable Vehicle Concepts" led at the Centre for ECO^2 Vehicle Design, a VinnExcellence Centre performing multi-vehicular multidisciplinary research to support a sustainable vehicle design development.

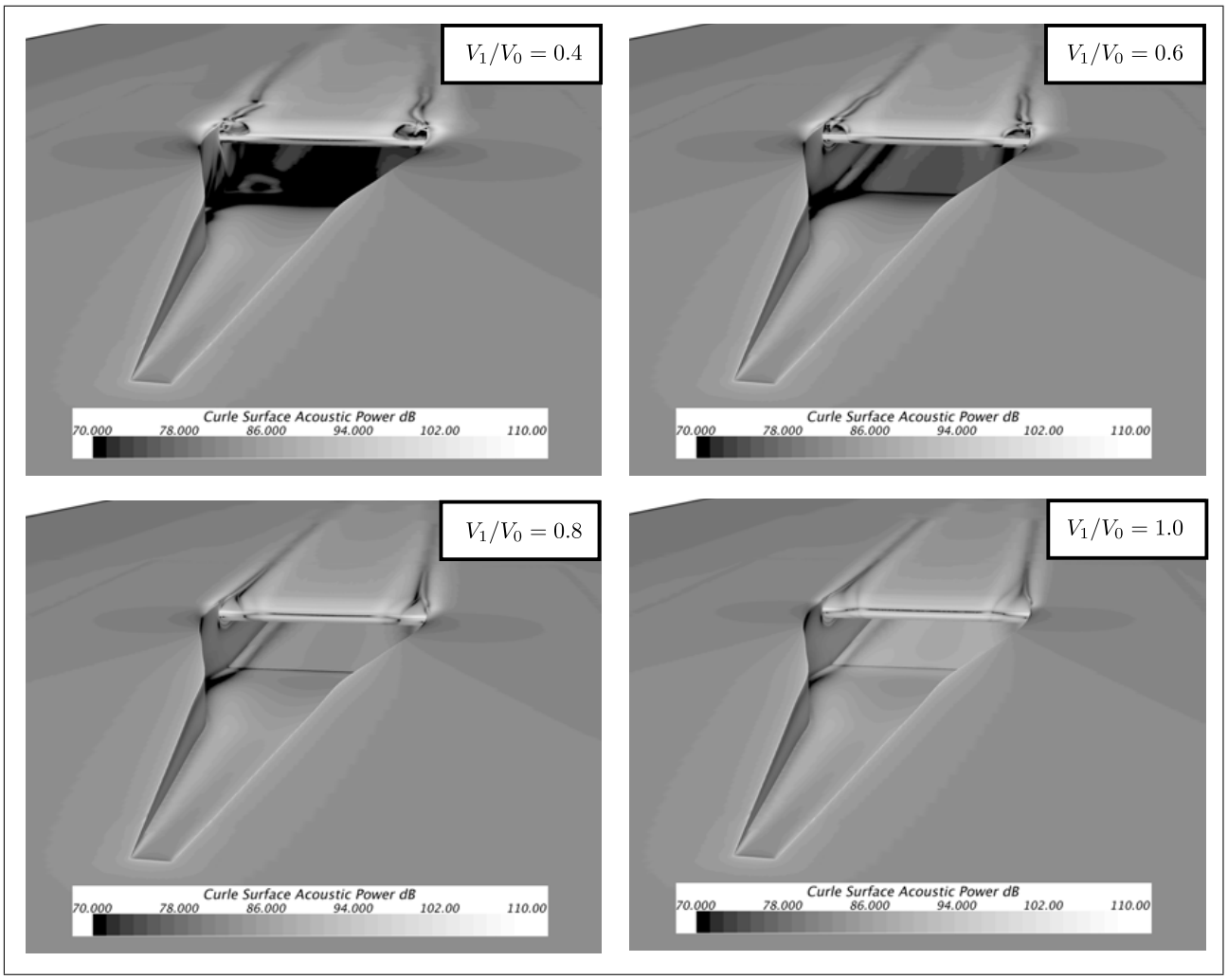

Figure 11. Broadband noise sources on the surface of the inlet.

References

[1] C. W. Frick, W. F. Davis, L. Randall, E. A. Mossman: An experimental investigation of NACA submerged-duct entrances. National Advisory Committee for Aeronautics Collection (1945).

[2] E. A. Mossman, L. M. Randall: An experimental investigation of the design variables for NACA submerged duct entrances. National Advisory Committee for Aeronautics Collection (1948).

[3] E. S. Taskinoglu, D. Knight: Numerical analysis of submerged inlets. AIAA Paper, Vol. 3147 (2002).

[4] S. Sun, R.-W. Guo: Numerical analysis and experimental validation of a submerged inlet on the plane surface. Chin. J. Aeronaut., Vol. 18, No. 3 (2005) 199-205.

[5] E. S. Taskinoglu, V. Jovanovic, D. Knight, G. Elliott: Design optimization for submerged inlets-Part II. 21st AIAA Appl. Aerodyn. Conf., Orlando, Florida, 2003, 23-26.

[6] E. S. Taskinoglu, V. Jovanovic, D. Knight, G. Elliott: Multi-objective design optimization and experimental measurements for a submerged inlet. 42nd AIAA Aerosp. Sci. Meet. Exhib, Reno, Nevada, 2004, 2004-2025.

[7] M. Siercke, U. Heise, J. Holmgren, A. Gommet: Air inlet for a vehicle. U.S. Patent No. 8,393,566, issued March 12, 2013.

[8] J. E. Ffowcs Williams, D. L. Hawkings: Sound generation by turbulence and surfaces in arbitrary motion. Philos. Trans. R. Soc., Ser. A, Math. Phys. Sci., Vol. 264, No. 1151 (1969) 321-342.

[9] STAR-CCM+, http://www.cd-adapco.com/products/star-ccm [Accessed: 2015-01-21]

[10] P. R. Spalart, S. R. Allmaras: A one-equation turbulence model for aerodynamic flows. Rech. Aérosp., **1** (1994) 5-21.

[11] F. R. Menter: Two-equation eddy-viscosity turbulence modeling for engineering applications. AIAA J., 32(8) (1994) 1598-1605.

[12] J. O. Hinze: Turbulence. McGraw-Hill, 1975, 672-673.